Title

Fabrication of Sealed Nanostraw Microdevices for Oral Drug Delivery

Journal

ACS Nano, 10(6)

ISSN

1936-0851

Authors

Fox, Cade B

Cao, Yuhong

Nemeth, Cameron L

et al.

Publication Date

2016-06-28

DOI

10.1021/acsnano.6b00809

Peer reviewed

HHS Public Access

Author manuscript

ACS Nano. Author manuscript; available in PMC 2017 May 17.

Published in final edited form as:

ACS Nano. 2016 June 28; 10(6): 5873–5881. doi:10.1021/acsnano.6b00809.

Fabrication of Sealed Nanostraw Microdevices for Oral Drug Delivery

Cade B. Fox[†], **Yuhong Cao**[‡], **Cameron L. Nemeth**[§], **Hariharasudhan D. Chirra**[†], **Rachel W. Chevalier**[†,||], **Alexander M. Xu**[‡,⊥], **Nicholas A. Melosh**[‡], and **Tejal A. Desai**[†,§,*]

[†]Department of Bioengineering and Therapeutic Sciences, University of California, San Francisco, California 94158, United States

[||]Department of Pediatrics, Division of Pediatric Gastroenterology, School of Medicine, University of California, San Francisco, California 94158, United States

[‡]Department of Materials Science and Engineering, Stanford University, Stanford, California 94305, United States

[§]Graduate Program in Bioengineering, University of California at Berkeley and San Francisco, UCSF Mission Bay Campus, San Francisco, California 94158, United States

Abstract

The oral route is preferred for systemic drug administration and provides direct access to diseased tissue of the gastrointestinal (GI) tract. However, many drugs have poor absorption upon oral administration due to damaging enzymatic and pH conditions, mucus and cellular permeation barriers, and limited time for drug dissolution. To overcome these limitations and enhance oral drug absorption, micron-scale devices with planar, asymmetric geometries, termed microdevices, have been designed to adhere to the lining of the GI tract and release drug at high concentrations directly toward GI epithelium. Here we seal microdevices with nanostraw membranes — porous nano-structured biomolecule delivery substrates — to enhance the properties of these devices. We demonstrate that the nanostraws facilitate facile drug loading and tunable drug release, limit the influx of external molecules into the sealed drug reservoir, and increase the adhesion of devices to epithelial tissue. These findings highlight the potential of nanostraw microdevices to enhance the oral absorption of a wide range of therapeutics by binding to the lining of the GI tract, providing prolonged and proximal drug release, and reducing the exposure of their payload to drug-degrading biomolecules.

Graphical abstract

[*]Corresponding Author: Tejal.Desai@ucsf.edu.

[⊥]Chemistry and Chemical Engineering Division, California Institute of Technology, Pasadena, CA 91125, United States.

The authors declare no competing financial interest.

Supporting Information

The Supporting Information is available free of charge on the ACS Publications website at DOI: 10.1021/acsnano.6b00809. Additional information on nanostraw microdevice fabrication, device profllometry data, and validation of device seal integrity following detachment from the silicon wafer (PDF)

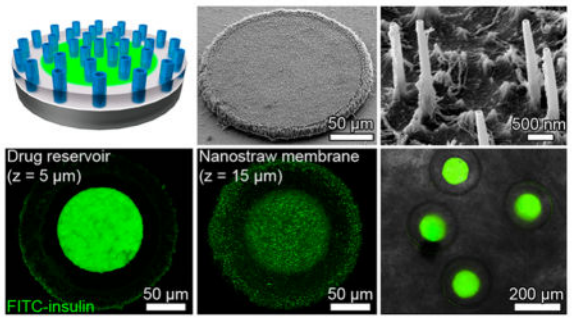

Keywords

microdevices; nanobiotechnology; nanostraws; nanowires; oral drug delivery

The oral route of drug administration is preferred due to its ease of use and low cost, but the physiological barriers of the GI tract prevent the absorption of intact biological therapeutics and many small molecule drugs. Specifically, metabolic and proteolytic enzymes present throughout the GI tract and the low pH of the stomach degrade drugs, and the intestinal epithelium and its adherent mucus layer limit permeation of drugs with high molecular weight or high polarity.[1–3] Additionally, many drugs exhibit low solubility and dissolve poorly within the small intestine, the primary site of systemic drug absorption.[1,2,4] Of such drugs with limited oral bioavailability, biological therapeutics are particularly challenging given their fragile nature and high molecular weights. However, some biological therapeutics currently require daily injections for periods of years to life (*e.g.*, insulin to treat diabetes, human growth hormone to treat growth hormone insufficiency, calcitonin and parathyroid hormone to treat osteoporosis)[5] and are thus highly desired candidates for oral drug delivery.

Micron-scale devices with planar, asymmetric geometries, termed microdevices, have been designed to address the barriers to oral drug absorption. Microdevices readily adhere to the lining of the GI tract for prolonged durations while releasing drug at high concentrations, thereby increasing drug permeation.[6] Microdevice bioadhesion is facilitated by the micron scale of the devices, which increases their surface-area-to-volume ratio, and the planar device geometry, which increases their interfacial surface area and decreases the force from fluid flow exerted on devices.[7,8] Furthermore, the asymmetric device design with the drug reservoir on only one side of the device can further enhance drug permeation; if the drug-releasing side of the device is selectively modified to have increased bioadhesion, then the devices can provide unidirectional release of drugs directly toward GI tissue.[9]

Microdevices are capable of significantly enhancing drug absorption both *in vitro* and *in vivo*.[7,8,10] However, loading drugs into the micron-scale reservoirs of these devices in a facile manner while also minimizing drug damage and achieving tunable and sustained drug release remains a challenge.[6] Additionally, incorporating nanotopography onto the surface of microdevices is likely to further enhance device bioadhesion by dramatically increasing their interfacial surface area, but developing fabrication approaches to coat microdevices with nanoscale features remains technically challenging.[6,11]

In this study, we enhance microdevice properties for oral drug delivery by incorporating nanostraw membrane caps. Nanostraws have been developed to facilitate the transport of nucleic acids, proteins, and drugs into cells for *in vitro* applications.[12–15] By piercing through membranes of seeded cells, nanostraws provide a pipeline for the diffusion of biomolecules directly into the cytosol.[12,15] Here, we develop an approach to fabricate planar microdevices with drug reservoirs sealed by nanostraw membranes and validate the structure and integrity of these devices. We go on to demonstrate that the nanostraws facilitate tunable and sustained drug release, limit the influx of outside biomolecules, and increase device bioadhesion. These findings indicate the potential of these devices to increase the oral absorption of a wide range of drugs with poor bioavailabilities. Furthermore, the fabrication approach presented here may be adapted to create other diagnostic and therapeutic devices where sealed microchambers with sustained release of biomolecules, protection of loaded reagents, and/or enhanced bioadhesion are required.

RESULTS AND DISCUSSION

To retain the planar, asymmetric microdevice design shown to enhance oral drug absorption, we designed the nanostraw microdevices to have circular bodies 200 μm in diameter with 100-μm-diameter drug reservoirs sealed by nanostraw membrane caps, with a total device thickness <20 μm. The devices were fabricated through a series of deposition, photolithography, and anisotropic etching steps as shown in Figure 1. First, an 8-μm-thick layer of poly(methyl methacrylate) (PMMA) followed by a layer of positive photoresist were spun cast onto a silicon wafer. The device body was then defined by exposing with UV light through a computer-designed photomask with arrays of opaque annuli (200 μm outer diameter, 100 μm inner diameter, 400 μm pitch) and subsequently developing the patterned photoresist (Figure 1A). The PMMA was anisotropically etched by approximately 5.5 μm with oxygen plasma (Supporting Information Figure S1) in regions not protected by the photoresist (Figure 1B). The remaining photoresist was chemically stripped, and the devices were briefly brought into contact with a polycaprolactone (PCL) film under heat, coating the topmost surface of the PMMA device bodies with a layer of PCL (Figure 1C).

To seal the device reservoirs, a nanostraw membrane composed of track-etched polycarbonate (PC) interspersed with vertically oriented aluminum oxide nanostraws was fabricated as previously described[15] and heat-bonded to the PCL (Figure 1D). The track etch membranes used to fabricate nanostraw membranes can be tuned for precise control over pore diameter and density, with pore diameters ranging from 8 nm to the millimeter scale and densities as high as 1×10^{10} cm^{-2}.[12,13,15–18] In this study, microdevices were sealed with nanostraw membranes ranging from 60 to 160 nm in inner nanostraw diameter and from 1×10^7 to 3×10^7 cm^{-2} in nanostraw density (drug release assays). For all other assays, devices were sealed with membranes with 60 nm inner nanostraw diameter and 1×10^7 cm^{-2} nanostraw density. To protect the nanostraw membrane during subsequent lithography steps, a sacrificial poly(vinyl alcohol) (PVA) layer was spun cast over the nanostraw membrane. A negative photoresist was spun cast over the PVA and exposed to UV light through an opaque photomask with 200 μm transparent circles aligned to the devices. The photoresist was then placed in developer, dissolving the photoresist in regions not cross-linked by UV exposure (Figure 1E). The regions of the nanostraw membrane and

PMMA not covered by the cross-linked photoresist were etched with oxygen plasma (Figure 1F), and the devices were rinsed in water to dissolve the PVA and release the photoresist caps (Figure 1G). The devices were then exposed to low-energy oxygen plasma to partially etch the PC, exposing the nanostraws (Figure 1H). Finally, the devices were incubated in concentrated drug solutions to load the device reservoirs *via* diffusion through nanostraws (Figure 1I). The final nanostraw microdevices were composed of PMMA, PCL, PC, and aluminum oxide, which are FDA-approved materials in various implanted biomedical devices.[19–22]

Scanning electron microscopy (SEM) demonstrated that nanostraw membrane caps were bound to the underlying PMMA device bodies (Figure 2A). The membranes had intact nanostraws measuring 2.2 ± 0.1 μm in length. While the distribution of nanostraws of membranes used in this study was stochastic on the nanometer scale, this distribution became more uniform on the cellular scale (Supporting Information Figure S2). This indicated that the nanostraw membranes would be capable of homogeneous transfer of drugs at the cellular and tissue scales.

To characterize the internal structure of the devices, we incubated the microdevices overnight in FITC-tagged bovine serum albumin (FITC-BSA), a protein known to have high adsorption to a variety of surfaces.[23] This step allowed the fluorescently labeled BSA to both diffuse into device reservoirs and adsorb onto the surfaces of the microdevices. The microdevices were then incubated in phosphate buffered saline (PBS) for 8 h to allow for partial FITC-BSA release, thereby reducing fluorescence intensity of FITC-BSA dissolved within the drug reservoirs and allowing both the drug reservoirs and the device surfaces to be visualized. Adhered and loaded FITC-BSA was then imaged with confocal fluorescence microscopy. While biomolecular adsorption was found to be minimal relative to the amount of dissolved drug within the device reservoirs (Supporting Information Figure S3), the adsorption of FITC-BSA to the surfaces of the devices (Figure 2B) indicated that the devices could be incubated in concentrated BSA in order to block adsorption of drugs loaded in later steps. This treatment could block adsorption of drugs found to adhere to device surfaces to increase the efficiency of drug release from device reservoirs.[24]

Z-slices of different depths showed the presence of drug reservoirs 100 μm in diameter with a surrounding device body and an overlying nanostraw membrane, both 200 μm in diameter (Figure 2B). Cross sections along the *z*-axis showed that nanostraws spanned through the membrane cap, connecting the device reservoirs to the external environment. Together, these findings suggested that loading of the microdevice reservoirs was mediated by diffusion of drug through the nanostraws.

Minimizing drug stress while loading microdevice reservoirs has proven challenging in previous studies. Current methods of microreservoir drug loading such as surface loading by capillary action,[25–28] photolithography,[8,10,29] and inkjet printing[30,31] require exposure of drug to UV light, cross-linking agents, organic solvents, and/or dehydration. These damaging conditions can potentially cause loss of drug structure and bioactivity, especially for biological therapeutics.[6] The nano-straw microdevices in this study were designed to facilitate in-solution drug loading, allowing drug to be loaded under mild conditions.

To confirm nanostraws as the route of drug diffusion into the device reservoirs and validate the integrity of device sealing, we fabricated devices with either nanostraw membrane caps or nonporous PC film caps as a control. Devices were then incubated overnight in a PBS solution of 10 mg/mL FITC-insulin, rinsed with PBS for 1 min, and imaged with fluorescence microscopy. FITC-insulin diffused into the reservoirs of devices with nanostraw membranes but not into the reservoirs of microdevices sealed with nonporous PC (Figure 3), demonstrating functional device reservoir sealing with drug diffusion occurring primarily through nanostraws. Additionally, drug-loaded microdevices retained FITC-insulin upon being scraped from the silicon wafer (Supporting Information Figure S4), indicating that the microdevices remained sealed upon device detachment.

In order to take full advantage of the prolonged residence time in the GI tract, bioadhesive microdevices should provide sustained drug release. Furthermore, an ability to tune the rate of drug release allows for targeting of specific regions of the GI tract and adjustment for more favorable pharmacokinetic profiles.[2] For example, rapid drug release could facilitate delivery of the majority of loaded drug to the buccal cavity, while slow release could maximize delivery of drug to the colon. We hypothesized that the hollow nanostraws, which can be fabricated with varying diameters and densities,[12–15] would provide the additional advantage of tunable and sustained drug release.

To test this hypothesis, we monitored the release rates of the model drug FITC-insulin from microdevices sealed by nanostraw caps of varying nanostraw inner diameters and densities (Figure 4A). For each type of nanostraw membrane, 400–800 microdevices were loaded by incubation in a PBS solution of 10 mg/mL FITC-insulin at 4 °C for 36–48 h. The microdevices were then rinsed in PBS for 1 min to remove nonloaded FITC-insulin and placed in PBS at 37 °C for measurement of drug release. The GI tract environment varies dramatically in composition, enzyme concentrations, and pH by region.[6] While drug release was performed in the absence of digestive enzymes to allow for the accurate measurement of drug concentrations, the pH at which drug release was tested (pH 7.4) falls within the pH ranges of the buccal cavity and esophagus (pH 5.3–7.8),[32] small intestine (pH 6–7.4),[33] and colon (pH 6.8–7.4)[34] but is significantly higher than the pH of the stomach (pH 1.0–3.5).[35] However, nanostraw micro-devices could be encapsulated within pH-sensitive enteric capsules in order to allow them to bypass the stomach before dissolution of the capsule and release of devices within the higher-pH environments of the intestine or colon.[6,36] Drug release was monitored by fluorescence spectroscopy, normalizing to device count (Figure 4B). Drug release rates scaled with both nanostraw diameter and density, demonstrating that drug release kinetics could be tuned by adjusting nanostraw membrane properties.

To mitigate drug degradation, microdevices can be designed to protect loaded drugs from exposure to damaging biomolecules such as metabolic and proteolytic enzymes that are present throughout the GI tract.[6] We hypothesized that, in addition to limiting diffusion of loaded drugs out of the reservoir, the nanostraw membrane would also limit the influx of outside biomolecules, thereby providing a mechanism to protect the drug payload. To model the diffusion of biomolecules into drug reservoirs, we incubated nanostraw microdevices (inner nanostraw diameter: 60 nm, nanostraw density: 1×10^7 cm^{-2}) in 1 mg/mL 10 kDa FITC-dextran, a biological molecule with a hydrodynamic radius (2.3 nm)[37] similar to drug-

degrading enzymes such as trypsin (1.9 nm),[38] chymotrypsin (2.5 nm),[39] and DNase I (2.5 nm).[40]

We monitored FITC-dextran diffusion into the device reservoirs at 0.5, 1, 2, and 4 h with confocal fluorescence microscopy (Figure 5). We then quantified the fluorescence intensity values within the device reservoirs. As a control for the concentration of FITC-dextran outside of the device reservoirs, fluorescence intensity was also measured at 48 h, by which time internal FITC-dextran concentration had equilibrated to that of the external environment (Supporting Information Figure S5). All earlier time points were normalized to the fluorescence intensity at this later time point, allowing for comparison between the concentration within the devices to the external concentration. During incubation in FITC-dextran, the normalized fluorescence intensity in device reservoirs remained below 50% of the 48 h control for over 2 h, suggesting that the nanostraw membrane will reduce the exposure of loaded drug to external biomolecules relative the outside concentration, especially within the first few hours of administration. As a reference for the rate of drug release from the reservoirs, we also monitored the release of FITC-insulin from nanostraw microdevices through identical methods, normalizing to initial FITC-insulin fluorescence intensity. We observed significant FITC-insulin release during the same time frame, demonstrating that nanostraw microdevices can decrease the exposure of loaded drug to outside biomolecules prior to release.

We hypothesized that the adhesive properties of micro-devices would be enhanced by the presence of nanostraws. To determine the effect of nanostraws on bioadhesion, micro-devices sealed with nanostraw membrane caps that had either been etched with oxygen plasma to expose nanostraws (depicted in Figure 1H) or not treated with the final etching step, resulting in control devices without exposed nanostraws (depicted in Figure 1G), were analyzed with a flow cell adhesion assay. Approximately 400 microdevices were detached from the silicon wafer and incubated in PBS over a monolayer of Caco-2 epithelial cells for 5 min with gentle shaking, facilitating contact between the nanostraw microdevices and the epithelial monolayer. A flow cell was then assembled over the microdevices, and a solution of porcine mucin was passed through the flow cell at increasing rates to achieve stepwise increments of fluid shear stress as previously outlined.[23,26,28,41]

We determined the fraction of microdevices remaining completely adhered to the Caco-2 monolayer following 5 min of flow at each shear stress value. Microdevices with exposed nanostraws demonstrated significantly higher adhesion than control microdevices (Figure 6A). Following exposure to fluid shear stress values increasing to 40 dyn/cm^2, 77 ± 7% of microdevices with exposed nanostraws and 33 ± 23% of microdevices without exposed nanostraws remained adhered, demonstrating that nanostraws dramatically enhance device bioadhesion. The high fraction of nanostraw microdevices remaining adhered also indicated that bound nanostraw microdevices are likely to remain attached to the intestinal epithelium while under physiological shear stress, which can range from 0.02 to 35 dyn/cm^2 during peristalsis.[42]

To characterize device interaction with the mucus layer coating intestinal epithelium, we performed an *ex vivo* adhesion assay with excised murine intestinal tissue. In an assay

adapted from previous studies,[43–46] we excised the jejunum from sacrificed mice and flowed devices suspended in oxygenated Tyrode's solution through the intestinal segment at 0.2 mL/min, a flow rate previously proposed for mice.[43,44,46] After 1 h of flow, we cut the jejunum longitudinally and used fluorescence microscopy to determine the number of devices remaining within the intestinal tissue and the number of devices that had flowed through the jejunum. Of the total devices counted, 87 ± 13% of the nanostraw devices remained within the intestinal segment after 1 h of flow, while only 51 ± 19% of the control device remained (Figure 6B). Fluorescence microscopy showed adhesion of intact insulin-loaded devices to the intestinal mucosa (Figure 6C).

SEM analysis of *ex vivo* tissue showed that 76% of 21 nanostraw microdevices observed were adhered in the orientation with the nanostraw membrane coming into contact with the intestinal tissue, as shown in Figure 6D, indicating that this binary event was nonrandom and selectively favored adhesion of the nanostraw membrane surface of the devices ($p < 0.05$). SEM imaging also demonstrated that the nanostraw membranes of the devices adhered to and became entrapped by the mucus layer. The enhanced mucoadhesion observed in the presence of nanostraws is likely due to penetration of nanostraws into the mucus, which could prevent device detachment by providing increased interfacial surface area and impeding lateral device movement. Therefore, an upper limitation of the residence time of these devices in the GI tract may be the turnover rate of the motile mucus in the small intestine, which is on the order of hours, unless the devices penetrate through this motile mucus layer to interact with the underlying epithelium, which has a turnover time on the order of days.[47–49] Thus, these devices are not likely to degrade before excretion from the GI tract, as they are composed of materials that degrade on the order of months or longer.[50–53] Furthermore, these devices could be tuned to release the majority of their drug payload within an hour (Supporting Information Figure S6), during which time the majority of devices remain bound to GI tissue in *ex vivo* studies, indicating that these devices could efficiently release their drug payload before passing through the GI tract. Together, the *in vitro* and *ex vivo* adhesion assays demonstrated that the nanostraws enhanced adhesion of the drug-releasing device surface to the intestinal epithelium while exposed to fluid flow, indicating that the nanostraws will facilitate prolonged and unidirectional drug release directly toward GI tissue.

CONCLUSION

To address the barriers to oral drug absorption, we present an approach to fabricate microdevices sealed with nanostraw membranes. These devices retain the planar, asymmetric geometry previously shown to enhance device adhesion and drug absorption. We demonstrate that nanostraw membranes incorporated into the microdevices provide the additional advantages of (1) facile, in-solution drug loading with sustained, tunable drug release; (2) limited influx of outside molecules into device reservoirs; and (3) nanotopography-mediated bioadhesion. Nanostraw microdevices have potential to increase oral drug absorption by binding to GI tissue, releasing drug at high local concentrations over a prolonged period of time, and reducing the exposure of their payload to drug-degrading biomolecules. Given their facile, in-solution drug loading mechanism and ability to limit the exposure of loaded drug to outside biomolecules, nanostraw microdevices may prove

particularly advantageous for fragile biological therapeutics. Thus, future *in vivo* studies will determine the ability of these microdevices to enhance the delivery of a wide range of hormones, nucleic acids, peptides, and proteins for either enhanced systemic absorption or local uptake into diseased GI tissue.

Even for drugs with high bioavailabilities, there is a strong motivation to develop devices capable of releasing drugs in the GI tract for prolonged periods of time to decrease dosing frequency, allowing for simplified dosing regimens and better patient adherence to therapies.[54] With high bioadhesion under physiological shear stress and tunable drug release rates, nanostraw microdevices have potential to significantly extend durations of systemic drug exposure. The fabrication approach presented here may also be applied outside the field of oral drug delivery to miniaturize implantable drug release systems, biosensors, and other biomedical devices where bioadhesion, tunable release, and/or protection of a payload from outside biomolecules are advantageous.

METHODS

Fabrication of Nanostraw Microdevices

The detailed methods for nanostraw microdevice fabrication are described in Supporting Information.

Scanning Electron Microscopy

Nonbiological samples were prepared for SEM by sputter coating with 8 nm of gold or iridium. Biological samples were prepared for SEM by fixing regions of tissue in 4% (w/v) paraformaldehyde in PBS followed by dehydration in a graded series of 20, 40, 60, 80, and 100% ethanol with 30 min of incubation at room temperature for each solution. Samples were stored in anhydrous ethanol at 4 °C overnight and then underwent critical point drying followed by sputter coating with 20 nm gold and iridium. Samples were imaged with a Carl Zeiss Ultra 55 field emission scanning electron microscope. Nanostraw diameters were measured to be 62 ± 3, 94 ± 5, 165 ± 9, (membranes fabricated with nanostraw densities of 1×10^7 cm^{-2}) and 86 ± 17 nm (membrane fabricated with a nanostraw density of 3×10^7 cm^{-2}) by analyzing SEM images with Fiji software.[55,56] Nanostraw lengths were measured with the same approach, accounting for the 45° imaging angle. All values in this study are reported with standard deviation.

Confocal Imaging of Internal Microdevice Structure

Micro-devices were incubated overnight at 4 °C in a PBS solution (pH 7.4) with 10 mg/mL FITC-BSA (Sigma-Aldrich) to load devices reservoirs with FITC-BSA and allow for adsorption of FITC-BSA to devices surfaces. The devices were then incubated at 37 °C in PBS for approximately 8 h to allow for partial release of FITC-BSA from device reservoirs for reduced fluorescence intensity during imaging. The devices were then imaged while submerged in PBS with a spectral confocal microscope with a 488 nm laser for excitation and a 525 nm emission filter. Z-stacks were captured at 1 μm intervals over the entire device structure. Fiji software was used to restack confocal images along the *z*-axis.

Reservoir Seal Integrity Assay

Microdevices fabricated using a nanostraw membrane (inner nanostraw diameter: 60 nm, nanostraw density: 1×10^7 cm^{-2}) or with a nonporous PC membrane were incubated in 10 mg/mL FITC-insulin (Sigma-Aldrich) in PBS overnight and rinsed with PBS. Microdevices were then submerged in PBS and imaged with bright-field microscopy to show device structure and fluorescence microscopy to observe FITC-insulin diffusion into device reservoirs.

Drug Release Assay

Silicon wafers with nanostraw microdevices were scored and broken into pieces approximately 1–2 cm^2 in area, and the microdevices on each piece were counted. The microdevices were then incubated in a PBS solution of 10 mg/mL FITC-insulin at 4 °C for 36–48 h, rinsed in PBS for 1 min, and placed in PBS at 37 °C. The PBS solution was sampled with complete buffer exchange at 0.25, 0.5, 1, 2, and 4 h. Drug concentrations were determined with fluorescence spectroscopy using a standard curve of serially diluted FITC-insulin, and the cumulative mass of released drug was normalized to device count.

Quantification of FITC-Dextran Permeation into Device Reservoirs

Nanostraw microdevices were incubated in a PBS solution of 1 mg/mL 10 kDa FITC-dextran (Sigma-Aldrich) at 37 °C. At 0.5, 1, 2, 4, and 48 h, microdevices were quickly rinsed in PBS and imaged with confocal fluorescence microscopy, collecting images with 2 μm z-steps over the entire device reservoirs. All samples were imaged under identical conditions while avoiding saturation of fluorescence signal. To allow for comparison between rates of influx of outside biomolecules and release of loaded drug, the fluorescence intensity of FITC-insulin loaded into microdevices at 10 mg/mL was also monitored at 0, 0.5, 1, 2, and 4 h through identical methods. The fluorescence intensity within device reservoirs was integrated for each time point with Fiji software. FITC-dextran fluorescence intensity was normalized to devices equilibrated with the outside FITC-dextran concentration (t = 48 h), and FITC-insulin fluorescence intensity was normalized to devices imaged immediately after FITC-insulin loading (t = 0 h).

Caco-2 Flow Cell Adhesion Assay

An epithelial flow cell adhesion assay was performed as previously outlined[23,26,28,41] with minor modifications. Briefiy, approximately 400 microdevices, with or without oxygen plasma etching to expose nanostraws (inner diameter: 60 nm, density: 10^7 cm^{-2}), were scraped from the silicon wafer with a razor, suspended in 1 mL PBS, and added to a monolayer of Caco-2 epithelial cells (ATCC) in a Petri dish. The microdevices were incubated over the cellular monolayer for 5 min under gentle shaking. A flow cell was then assembled over the microdevices, and a solution of 20 g/L porcine mucin (Sigma-Aldrich) in PBS was passed through the flow cell at increasing flow rates in a stepwise fashion, achieving fluid shear stress values of 0.5, 1, 5, 10, 20, and 40 dyn/cm^2. After 5 min at each flow rate, the number of completely adhered microdevices (*i.e.*, the number of microdevices lying flat on the Caco-2 monolayer) was determined by counting under a dissecting

microscope, and the ratio of microdevices adhered to the original number of microdevices was determined.

Ex Vivo Adhesion Assay

An *ex vivo* nanostraw microdevice adhesion assay was adapted from previous protocols.[43–46] Six C57BL/6 mice (Jackson Laboratories, maintained in specific pathogen-free conditions) were sacrificed at 4–6 weeks of age, and the jejunum was excised. The intestinal segments were flushed with oxygenated Tyrode's solution (pH 6.8) to clear intestinal contents and confirm the absence of punctures, and the tissue was stored in oxygenated Tyrode's solution on ice until use within 4 h. For each sample, a jejunum segment was placed in a 37 °C bath of oxygenated Tyrode's solution. A 1–2 cm^2 piece of silicon wafer with approximately 400–800 nanostraw microdevices or control devices without exposed nanostraws (all loaded with 10 mg/mL FITC-insulin and washed in PBS for 1 min as previously described) was coated with 100 μL oxygenated Tyrode's solution, and devices were scraped from the surface of the silicon wafer with a razor. The suspended devices were slowly pipetted into the oral side of the jejunum and then flowed through the jejunum in oxygenated Tyrode's solution at 0.2 mL/min *via* a peristaltic pump. The buffer flowing out of the jejunum was passed through a metal grid with 70 μm spacing to collect detached devices. After 1 h of flow, the jejunum was cut longitudinally and placed between glass slides. The number of devices remaining within the jejunum and the number of devices collected in the metal grid were counted *via fl*uorescence microscopy, and the percentage of devices remaining attached to the jejunum was calculated for each sample.

Supplementary Material

Refer to Web version on PubMed Central for supplementary material.

Acknowledgments

C.B.F. was supported by NIH Training Grant 5T32GM007175-37 and an ARCS Fellowship. Y.C. was supported by Grant 70NANB15H192 from the U.S. Department of Commerce, National Institute of Standards and Technology. C.L.N. was supported by NSF Graduate Research Fellowship DGE-1106400. R.W.C. was supported by NIH Training Grant 5T32DK007762-38. A.M.X. was supported by NSF Graduate Fellowship DGE-114747 and an NDSEG Fellowship. This work was partially supported by NIH grant R01EB018842. We gratefully acknowledge use of the Carl Zeiss Ultra FE-SEM at San Francisco State University for all SEM imaging. The FE-SEM and supporting facilities were obtained under NSF-MRI award no. 0821619 and NSF-EAR award no. 0949176. Confocal fluorescence imaging was conducted at the Nikon Imaging Center, UCSF. Nanostraw membrane fabrication was performed the Stanford Nano Shared Facilities. Remaining fabrication was performed at the UCSF Biomedical Micro & Nanotechnology Core and UC Berkeley Biomolecular Nanotechnology Center. The authors would like to thank Colin Zamecnik, Margaret Lowe, and Jessie Lee for providing mouse tissue for the *ex vivo* experiments.

References

1. Patel VF, Liu F, Brown MB. Advances in Oral Transmucosal Drug Delivery. J Controlled Release. 2011; 153:106–116.
2. Chirra HD, Desai TA. Emerging Microtechnologies for the Development of Oral Drug Delivery Devices. Adv Drug Delivery Rev. 2012; 64:1569–1578.
3. Chaturvedi K, Ganguly K, Nadagouda MN, Aminabhavi TM. Polymeric Hydrogels for Oral Insulin Delivery. J Controlled Release. 2013; 165:129–138.

4. Thanki K, Gangwal RP, Sangamwar AT, Jain S. Oral Delivery of Anticancer Drugs: Challenges and Opportunities. J Controlled Release. 2013; 170:15–40.
5. Park K, Kwon IC, Park K. Oral Protein Delivery: Current Status and Future Prospect. React Funct Polym. 2011; 71:280–287.
6. Fox CB, Kim J, Le LV, Nemeth CL, Chirra HD, Desai TA. Micro/Nanofabricated Platforms for Oral Drug Delivery. J Controlled Release. 2015; 219:431–444.
7. Chirra HD, Shao L, Ciaccio N, Fox CB, Wade JM, Ma A, Desai TA. Planar Microdevices for Enhanced *In Vivo* Retention and Oral Bioavailability of Poorly Permeable Drugs. Adv Healthcare Mater. 2014; 3:1648–1654.
8. Ainslie KM, Lowe RD, Beaudette TT, Petty L, Bachelder EM, Desai TA. Microfabricated Devices for Enhanced Bioadhesive Drug Delivery: Attachment to and Small-Molecule Release through a Cell Monolayer under Flow. Small. 2009; 5:2857–2863. [PubMed: 19787677]
9. Tao SL, Desai TA. Micromachined Devices: The Impact of Controlled Geometry from Cell-Targeting to Bioavailability. J Controlled Release. 2005; 109:127–138.
10. Chirra HD, Desai TA. Multi-Reservoir Bioadhesive Microdevices for Independent Rate-Controlled Delivery of Multiple Drugs. Small. 2012; 8:3839–3846. [PubMed: 22962019]
11. Walsh LA, Allen JL, Desai TA. Nanotopography Applications in Drug Delivery. Expert Opin Drug Delivery. 2015; 12:1823–1827.
12. Xu AM, Aalipour A, Leal-Ortiz S, Mekhdjian AH, Xie X, Dunn AR, Garner CC, Melosh NA. Quantification of Nanowire Penetration into Living Cells. Nat Commun. 2014; 5:3613. [PubMed: 24710350]
13. Xie X, Xu AM, Leal-Ortiz S, Cao Y, Garner CC, Melosh NA. Nanostraw-Electroporation System for Highly Efficient Intracellular Delivery and Transfection. ACS Nano. 2013; 7:4351–4358. [PubMed: 23597131]
14. Xie X, Aalipour A, Gupta SV, Melosh NA. Determining the Time Window for Dynamic Nanowire Cell Penetration Processes. ACS Nano. 2015; 9:11667–11677. [PubMed: 26554425]
15. VanDersarl JJ, Xu AM, Melosh NA. Nanostraws for Direct Fluidic Intracellular Access. Nano Lett. 2012; 12:3881–3886. [PubMed: 22166016]
16. Spende A, Sobel N, Lukas M, Zierold R, Riedl JC, Gura L, Schubert I, Moreno JM, Nielsch K, Stuhn B, Hess C, Trautmann C, Toimil-Molares ME. TiO_2, SiO_2, and Al_2O_3 Coated Nanopores and Nanotubes Produced by ALD in Etched Ion-Track Membranes for Transport Measurements. Nanotechnology. 2015; 26:335301. [PubMed: 26225468]
17. Chakarvarti SK. Track-Etch Membranes Enabled Nano-/Microtechnology: A Review. Radiat Meas. 2009; 44:1085–1092.
18. Williams WD, Giordano N. Fabrication of 80-Å Metal Wires. Rev Sci Instrum. 1984; 55:410–412.
19. Wang Q, Webster TJ. Nanostructured Selenium for Preventing Biofilm Formation on Polycarbonate Medical Devices. J Biomed Mater Res, Part A. 2012; 100A:3205–3210.
20. Shimko DA, Nauman EA. Development and Characterization of a Porous Poly(Methyl Methacrylate) Scaffold with Controllable Modulus and Permeability. J Biomed Mater Res, Part B. 2007; 80B:360–369.
21. Nyitray CE, Chang R, Faleo G, Lance KD, Bernards DA, Tang Q, Desai TA. Polycaprolactone Thin-Film Micro- and Nanoporous Cell-Encapsulation Devices. ACS Nano. 2015; 9:5675–5682. [PubMed: 25950860]
22. Masson B. Emergence of the Alumina Matrix Composite in Total Hip Arthroplasty. Int Orthop. 2009; 33:359–363. [PubMed: 18043920]
23. Jeyachandran YL, Mielczarski E, Rai B, Mielczarski JA. Quantitative and Qualitative Evaluation of Adsorption/Desorption of Bovine Serum Albumin on Hydrophilic and Hydrophobic Surfaces. Langmuir. 2009; 25:11614–11620. [PubMed: 19788219]
24. Jeyachandran YL, Mielczarski JA, Mielczarski E, Rai B. Efficiency of Blocking of Non-Specific Interaction of Different Proteins by BSA Adsorbed on Hydrophobic and Hydrophilic Surfaces. J Colloid Interface Sci. 2010; 341:136–142. [PubMed: 19818963]
25. Fox CB, Kim J, Schlesinger EB, Chirra HD, Desai TA. Fabrication of Micropatterned Polymeric Nanowire Arrays for High-Resolution Reagent Localization and Topographical Cellular Control. Nano Lett. 2015; 15:1540–1546. [PubMed: 25639724]

26. Fischer KE, Nagaraj G, Hugh Daniels R, Li E, Cowles VE, Miller JL, Bunger MD, Desai TA. Hierarchical Nanoengineered Surfaces for Enhanced Cytoadhesion and Drug Delivery. Biomaterials. 2011; 32:3499–3506. [PubMed: 21296409]
27. Fischer KE, Jayagopal A, Nagaraj G, Daniels RH, Li EM, Silvestrini MT, Desai TA. Nanoengineered Surfaces Enhance Drug Loading and Adhesion. Nano Lett. 2011; 11:1076–1081. [PubMed: 21280638]
28. Fischer KE, Aleman BJ, Tao SL, Daniels RH, Li EM, Bunger MD, Nagaraj G, Singh P, Zettl A, Desai TA. Biomimetic Nanowire Coatings for Next Generation Adhesive Drug Delivery Systems. Nano Lett. 2009; 9:716–720. [PubMed: 19199759]
29. Ainslie KM, Kraning CM, Desai TA. Microfabrication of an Asymmetric, Multi-Layered Microdevice for Controlled Release of Orally Delivered Therapeutics. Lab Chip. 2008; 8:1042–1047. [PubMed: 18584077]
30. Marizza P, Keller SS, Mullertz A, Boisen A. Polymer-Filled Microcontainers for Oral Delivery Loaded Using Supercritical Impregnation. J Controlled Release. 2014; 173:1–9.
31. Fujie T, Desii A, Ventrelli L, Mazzolai B, Mattoli V. Inkjet Printing of Protein Microarrays on Freestanding Polymeric Nanofilms for Spatio-Selective Cell Culture Environment. Biomed Microdevices. 2012; 14:1069–1076. [PubMed: 22986760]
32. Humphrey SP, Williamson RT. A Review of Saliva: Normal Composition, Flow, and Function. J Prosthet Dent. 2001; 85:162–169. [PubMed: 11208206]
33. Fallingborg J. Intraluminal pH of the Human Gastrointestinal Tract. Dan Med Bull. 1999; 46:183–196. [PubMed: 10421978]
34. Fallingborg J, Christensen LA, Jacobsen BA, Rasmussen SN. Very Low Intraluminal Colonic pH in Patients with Active Ulcerative Colitis. Dig Dis Sci. 1993; 38:1989–1993. [PubMed: 8223071]
35. Yoshida T, Lai TC, Kwon GS, Sako K. pH- and Ion-Sensitive Polymers for Drug Delivery. Expert Opin Drug Delivery. 2013; 10:1497–1513.
36. Al-Hilal TA, Alam F, Byun Y. Oral Drug Delivery Systems Using Chemical Conjugates or Physical Complexes. Adv Drug Delivery Rev. 2013; 65:845–864.
37. Watson PM, Paterson JC, Thom G, Ginman U, Lundquist S, Webster CI. Modelling the Endothelial Blood-CNS Barriers: A Method for the Production of Robust *In Vitro* Models of the Rat Blood-Brain Barrier and Blood-Spinal Cord Barrier. BMC Neurosci. 2013; 14:59. [PubMed: 23773766]
38. Chiu K, Agoubi LL, Lee I, Limpar MT, Lowe JW Jr, Goh SL. Effects of Polymer Molecular Weight on the Size, Activity, and Stability of PEG-Functionalized Trypsin. Biomacromolecules. 2010; 11:3688–3692. [PubMed: 20979350]
39. Antosiewicz J, Porschke D. The Nature of Protein Dipole Moments: Experimental and Calculated Permanent Dipole of Alpha-Chymotrypsin. Biochemistry. 1989; 28:10072–10078. [PubMed: 2620062]
40. Lizarraga B, Sanchez-Romero D, Gil A, Melgar E. The Role of Ca^{2+} on pH-Induced Hydrodynamic Changes of Bovine Pancreatic Deoxyribonuclease A. J Biol Chem. 1978; 253:3191–3195. [PubMed: 25282]
41. Mikos AG, Peppas NA. Bioadhesive Analysis of Controlled-Release Systems. IV. An Experimental Method for Testing the Adhesion of Microparticles with Mucus. J Controlled Release. 1990; 12:31–37.
42. Marzorati M, Vanhoecke B, De Ryck T, Sadaghian Sadabad M, Pinheiro I, Possemiers S, Van den Abbeele P, Derycke L, Bracke M, Pieters J, Hennebel T, Harmsen HJ, Verstraete W, Van de Wiele T. The HMI Module: A New Tool to Study the Host-Microbiota Interaction in the Human Gastrointestinal Tract *In Vitro*. BMC Microbiol. 2014; 14:133. [PubMed: 24884540]
43. Wang B, Mao YK, Diorio C, Pasyk M, Wu RY, Bienenstock J, Kunze WA. Luminal Administration *Ex Vivo* of a Live Lactobacillus Species Moderates Mouse Jejunal Motility within Minutes. FASEB J. 2010; 24:4078–4088. [PubMed: 20519636]
44. Mols R, Brouwers J, Schinkel AH, Annaert P, Augustijns P. Intestinal Perfusion with Mesenteric Blood Sampling in Wild-Type and Knockout Mice: Evaluation of a Novel Tool in Biopharmaceutical Drug Profiling. Drug Metab Dispos. 2009; 37:1334–1337. [PubMed: 19273528]

45. Luo Z, Liu Y, Zhao B, Tang M, Dong H, Zhang L, Lv B, Wei L. *Ex Vivo* and *In Situ* Approaches Used to Study Intestinal Absorption. J Pharmacol Toxicol Methods. 2013; 68:208–216. [PubMed: 23831587]
46. Escribano E, Sala XG, Salamanca J, Navarro CR, Regue JQ. Single-Pass Intestinal Perfusion to Establish the Intestinal Permeability of Model Drugs in Mouse. Int J Pharm. 2012; 436:472–477. [PubMed: 22814225]
47. Wu L, Liu M, Zhu X, Shan W, Huang Y. Modification Strategies of Lipid-Based Nanocarriers for Mucosal Drug Delivery. Curr Pharm Des. 2015; 21:5198–5211. [PubMed: 26412355]
48. Ermund A, Schutte A, Johansson ME, Gustafsson JK, Hansson GC. Studies of Mucus in Mouse Stomach, Small Intestine, and Colon. I. Gastrointestinal Mucus Layers Have Different Properties Depending on Location as Well as over the Peyer's Patches. Am J Physiol Gastrointest Liver Physiol. 2013; 305:G341–G347. [PubMed: 23832518]
49. Gunther C, Buchen B, Neurath MF, Becker C. Regulation and Pathophysiological Role of Epithelial Turnover in the Gut. Semin Cell Dev Biol. 2014; 35:40–50. [PubMed: 24973733]
50. Wong HM, Zhao Y, Tam V, Wu S, Chu PK, Zheng Y, To MK, Leung FK, Luk KD, Cheung KM, Yeung KW. *In Vivo* Stimulation of Bone Formation by Aluminum and Oxygen Plasma Surface-Modified Magnesium Implants. Biomaterials. 2013; 34:9863–9876. [PubMed: 24060425]
51. Bolgen N, Menceloglu YZ, Acatay K, Vargel I, Piskin E. *In Vitro* and *In Vivo* Degradation of Non-Woven Materials Made of Poly(Epsilon-Caprolactone) Nanofibers Prepared by Electrospinning under Different Conditions. J Biomater Sci, Polym Ed. 2005; 16:1537–1555. [PubMed: 16366336]
52. Ayre WN, Denyer SP, Evans SL. Ageing and Moisture Uptake in Polymethyl Methacrylate (PMMA) Bone Cements. J Mech Behav Biomed Mater. 2014; 32:76–88. [PubMed: 24445003]
53. Arjun GN, Ramesh P. Structural Characterization, Mechanical Properties, and *In Vitro* Cytocompatibility Evaluation of Fibrous Polycarbonate Urethane Membranes for Biomedical Applications. J Biomed Mater Res, Part A. 2012; 100A:3042–3050.
54. Traverso G, Langer R. Perspective: Special Delivery for the Gut. Nature. 2015; 519:S19. [PubMed: 25806494]
55. Schneider CA, Rasband WS, Eliceiri KW. NIH Image to Image J: 25 Years of Image Analysis. Nat Methods. 2012; 9:671–675. [PubMed: 22930834]
56. Schindelin J, Arganda-Carreras I, Frise E, Kaynig V, Longair M, Pietzsch T, Preibisch S, Rueden C, Saalfeld S, Schmid B, Tinevez JY, White DJ, Hartenstein V, Eliceiri K, Tomancak P, Cardona A. Fiji: An Open-Source Platform for Biological-Image Analysis. Nat Methods. 2012; 9:676–682. [PubMed: 22743772]

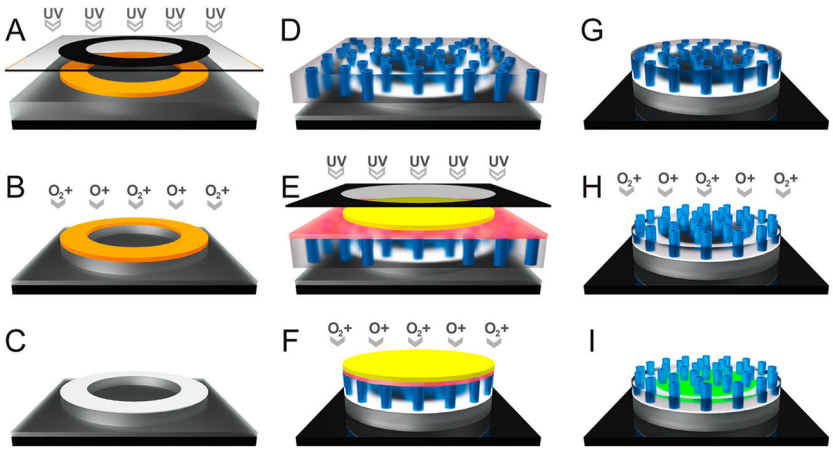

Figure 1.

Nanostraw microdevice fabrication schematic. (A) A silicon wafer (black) is spun cast with 1) PMMA (gray) and 2) positive photoresist (orange), and the photoresist is patterned *via* UV exposure through a computer-designed photomask with subsequent development. (B) The PMMA layer is partially etched with oxygen plasma to form the device body. (C) Following chemical removal of remaining photoresist, PCL (white) is transferred onto the surface of the devices by contact under heat. (D) The devices are heat-bonded to a nanostraw membrane composed of PC (semitransparent) interspersed with aluminum oxide nanostraws (blue), sealing the devices. (E) The nanostraw membrane is spun cast with (1) PVA (red) and (2) negative photoresist (yellow), which is patterned over the devices *via* UV exposure through a photomask with subsequent development. (F) The nanostraw membrane and PMMA are removed in regions not protected by the patterned photoresist by etching with oxygen plasma. (G) The photoresist caps are detached by dissolving the underlying PVA layer in water. (H) The polycarbonate is partially etched with oxygen plasma to expose the alumina nanostraws. (I) Following incubation in a drug solution to facilitate drug loading *via* diffusion through nanostraws, the device reservoirs contain high concentrations of drug (green).

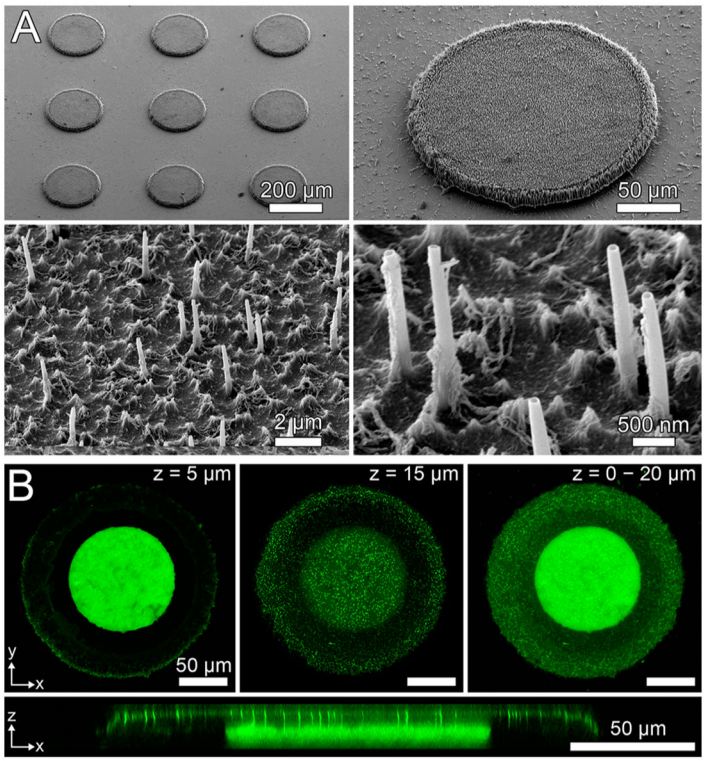

Figure 2.

Characterization of nanostraw microdevice structure. (A) SEM images demonstrate that microdevices were fabricated with intact nanostraw membranes. (B) Confocal fluorescence microscopy of nanostraw devices incubated in a FITC-BSA solution and imaged while submerged in PBS provides visualization of the drug reservoir ($z = 5\ \mu m$), the overlying nanostraw membrane ($z = 15\ \mu m$), and overall device structure ($z = 0–20\ \mu m$). An $x–z$ cross section shows that nanostraws provide a fluidic conduit for drug diffusion between device reservoirs and the external environment.

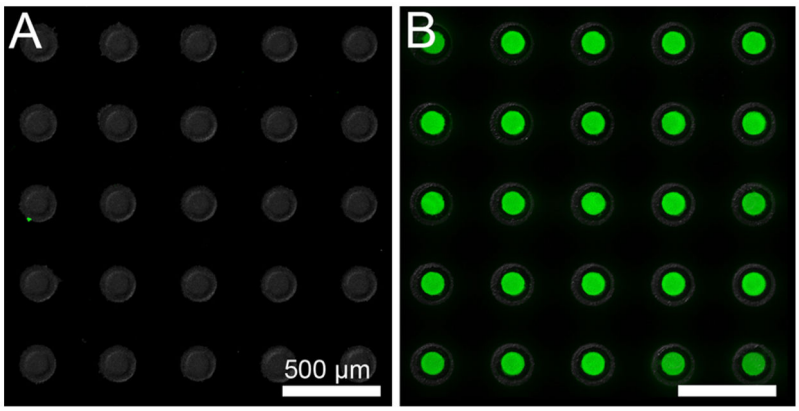

Figure 3.

Nanostraw microdevice reservoirs are sealed, with nanostraws facilitating in-solution drug loading. Microdevices fabricated using (A) a nonporous PC membrane or (B) a nanostraw membrane were incubated in 10 mg/mL FITC-insulin overnight, rinsed with PBS, and imaged for device structure (bright-field signal, shown in grayscale) and FITC-insulin localization (fluorescence signal, shown in green). Only microdevices with nanostraws showed significant loading of insulin into reservoirs, indicating proper sealing of microdevices with drug diffusion occurring primarily through nanostraws.

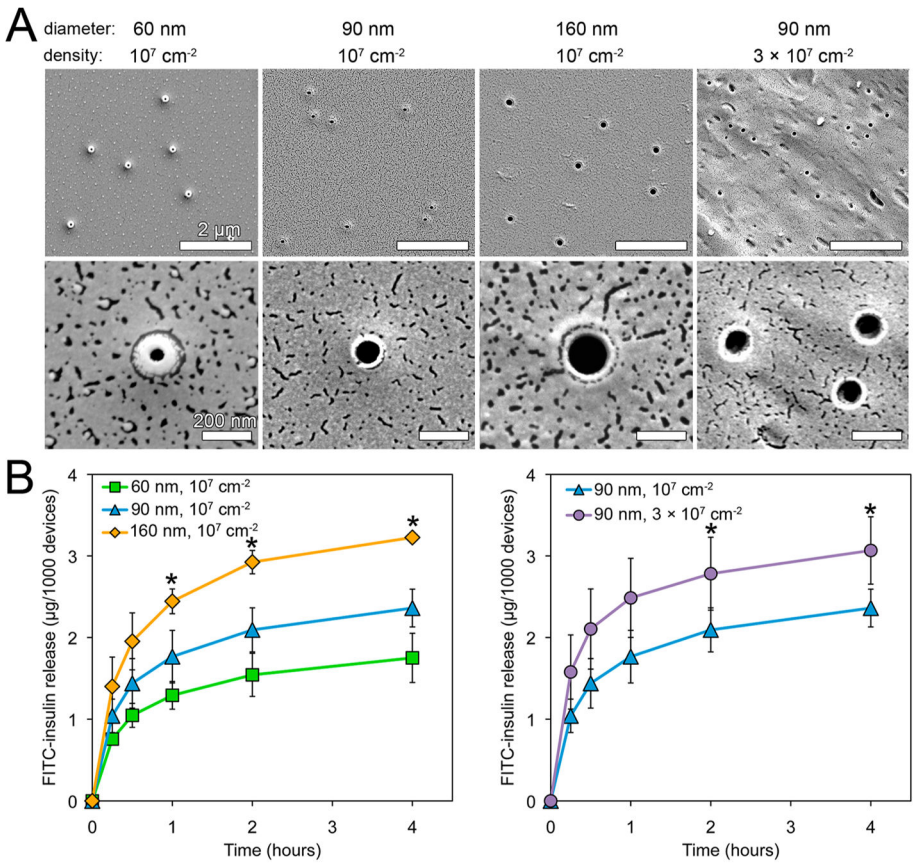

Figure 4.

Drug release rates scale with nanostraw diameter and density, allowing for tunable release. (A) SEM images of nanostraw membranes fabricated with varying nanostraw inner diameters (60, 90, 160 nm) and densities (1×10^7, 3×10^7 cm^{-2}). (B) FITC-insulin release from microdevices sealed with these membranes was monitored over time. Release rates scaled with both nanostraw diameter and density. *Indicates statistically different values between all samples at a given time point ($p < 0.05$).

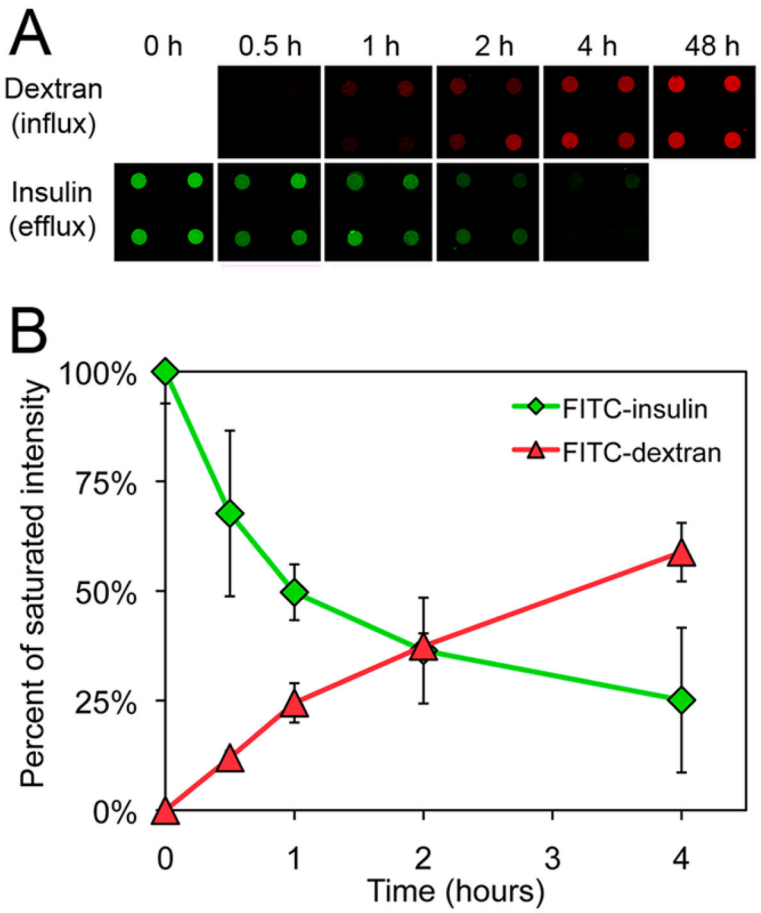

Figure 5.

Nanostraw membranes limit the influx of biomolecules into device reservoirs. (A) To determine the ability of nanostraw microdevices to limit the influx of outside biomolecules, nanostraw microdevices were incubated in 1 mg/mL 10 kDa FITC-dextran at 37 °C and imaged with confocal fluorescence microscopy over time. As a reference for the rate of drug release from the reservoirs, the release of FITC-insulin loaded into microdevices at 10 mg/mL was also monitored through identical detection methods. (B) FITC-dextran influx and FITC-insulin eflux were quantified by integrating fluorescence intensity values in the device reservoirs at each time point and normalizing to the respective saturated intensity values. Specifically, FITC-dextran fluorescence intensity was normalized to devices equilibrated with the outside FITC-dextran concentration (t = 48 h), and FITC-insulin fluorescence intensity was normalized to loaded devices (t = 0 h).

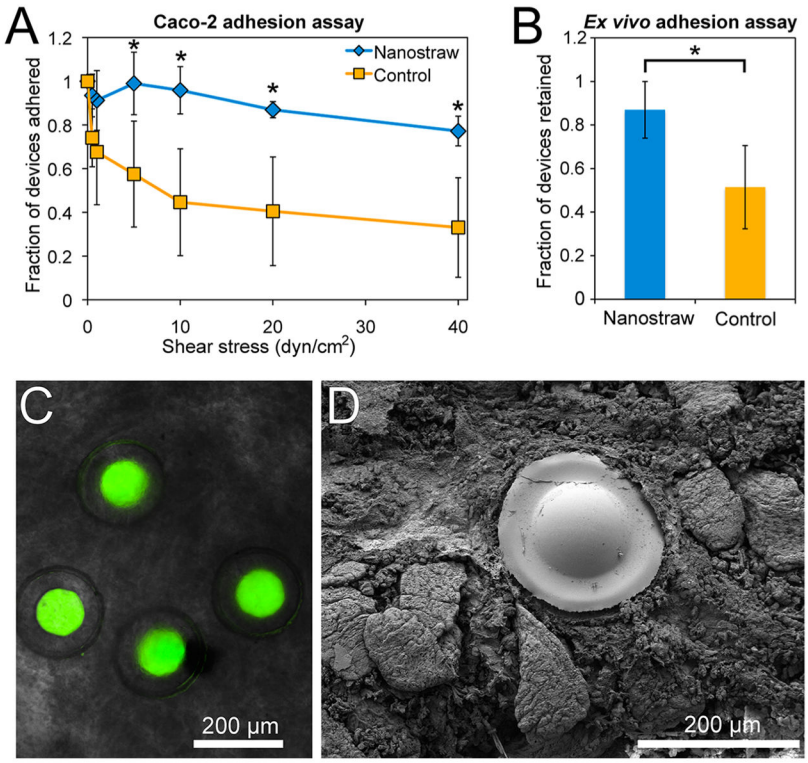

Figure 6.

Nanostraws enhance microdevice bioadhesion. (A) *In vitro flo*w cell assay in which nanostraw microdevices or control devices sealed with membranes lacking exposed nanostraws were incubated on Caco-2 cells and then exposed to increasing flow rates corresponding to physiological fluid shear stress values. The fraction of devices remaining adhered to the Caco-2 monolayer was determined at each time point. (B) *Ex vivo* murine intestinal adhesion assay in which nanostraw microdevices or control devices were flowed through excised murine intestinal tissue at 0.2 mL/min for 1 h. The fraction of devices remaining within the intestinal tissue was then determined with fluorescence microscopy. (C) Fluorescence microscopy following the *ex vivo* adhesion assay showed that intact nanostraw microdevices loaded with FITC-insulin (green) had adhered to intestinal tissue. (D) An SEM image showing a microdevice adhered to the intestine as a result of the nanostraw membrane becoming entrapped within the mucus layer. 76% of devices observed by SEM were adhered with the nanostraw membrane in contact with the intestinal mucosa ($n = 21$), indicating that devices selectively bound in this orientation ($p < 0.05$). *Indicates statistically different values ($p < 0.05$).